Marine Geology 470 (2024) 107270

Contents lists available at ScienceDirect

Marine Geology

journal homepage: www.elsevier.com/locate/margo

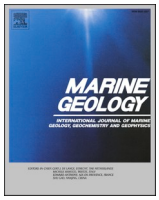

Research Article

A tale of a changing basin - a transient model of the 7.17 event leading to the Messinian Salinity Crisis

Ronja M. Ebner [a,*], Francesca Bulian [b,c], Francisco J. Sierro [b], Tanja J. Kouwenhoven [a], Paul Th. Meijer [a]

[a] Department of Earth Sciences, Utrecht University, The Netherlands
[b] Department de Geología, Univ. de Salamanca, Plaza de los Caídos s/n, 37008 Salamanca, Spain
[c] University of Groningen, Groningen Institute of Archaeology, Poststraat 6, 9712 ER Groningen, The Netherlands

ARTICLE INFO

Editor: Shu Gao

Keywords:
Box model
Convection
Mediterranean Sea
Messinian Salinity Crisis
Gateway
Closure
Semi-enclosed sea

ABSTRACT

Before the Messinian Salinity Crisis (MSC) left its imprint on the sediment record of the Mediterranean Sea in the form of evaporites, the basin had already undergone significant changes. At 7.17 Ma, a drop in δ13C values, as well as a basin-wide shift in the abundance of benthic foraminifers, already attest to a sudden change in the Mediterranean conditions.

This event coincides with an increase in the amplitude of the insolation curve. It thus stands to question whether a change in the freshwater budget or a change in the connection between the Mediterranean Sea and the Atlantic was the driver for this event. Answering this question would not only help to understand the event itself, but might also help to decipher the early dynamics of the MSC.

With a computational box model, we investigate the response of the Mediterranean Sea to a varying freshwater budget for a wide range of restriction. The results then let us define scenarios in which we analyse how a gradually changing restriction would express itself in the basin dynamics.

We find that the change in the freshwater budget alone cannot explain the changes that are attributed with the 7.2 event, but coupled with an increase in restriction most differences can be accounted for. Our results also show that a gradual change in restriction can provoke a non-linear response in the behaviour of the basin, which can appear abrupt when happening on a short enough timescale. Such a change would also enhance the influence of said changes in the freshwater budget.

This tells us that the processes that most likely triggered the Messinian Salinity Crisis started much earlier and incrementally increased the restriction of the Mediterranean Sea.

1. Introduction

While, since 14 Ma, ocean connections between the Mediterranean and the Indo-Pacific Ocean remained closed and those with the Paratethys (Adams et al., 1983; Barrier and Vrielynck, 2008; Rögl, 1999) were only short-lived (Krijgsman et al., 2010; Stoica et al., 2016), the primary connection of the Mediterranean with the world ocean was via gateways to the Atlantic (e.g. Flecker et al., 2015 and references therein). During this time, the Mediterranean-Atlantic exchange was taking place most probably through the Betic and Rifian corridors, situated in southern Spain and northern Morocco (e.g. Benson et al., 1992; Capella et al., 2018; Krijgsman et al., 1999; Van Assen et al., 2006). For a concentration basin like the Mediterranean Sea, such a connection is fundamental to compensate the freshwater deficit, which would otherwise lead to a rapid sea level drawdown. Around 7–8 Ma, tectonic activity caused uplift of the Betics (Garcia-Castellanos and Villaseñor, 2011; Govers, 2009; Mancilla et al., 2015), restricting the seaways of the Betic and Rifian corridors and Gibraltar Arc (Fadil et al., 2006; Tulbure et al., 2017; Van den Berg et al., 2018) and culminating in the extraordinary paleoenvironmental event known as the Messinian Salinity Crisis (MSC; 5.96–5.33 Ma; CIESM, 2008; Flecker et al., 2015; Roveri et al., 2014; Selli, 1964).

Given the importance of the connection with the Atlantic Ocean and in order to better understand which changes at the corridors affected the basin and how, many studies on sediments both on the Mediterranean and Atlantic side of the Gibraltar Arc gateways have been performed in

* Corresponding author.
E-mail address: r.m.ebner@uu.nl (R.M. Ebner).

https://doi.org/10.1016/j.margeo.2024.107270
Received 30 June 2023; Received in revised form 11 February 2024; Accepted 11 March 2024
Available online 16 March 2024

the last decades (Booth-Rea et al., 2018; Bulian et al., 2021; Martín et al., 1999; Van den Berg et al., 2018; Van Der Laan et al., 2012; Van Der Schee et al., 2016). Offshore, seismic data acquired all over the Mediterranean Basin, enabled the mapping of the Messinian evaporites (e.g. Lofi et al., 2011). If only because of the technical problems related to the drilling of such deposits and the consequent impossibility to acquire a continuous deep MSC record, numerical models have been used as a tool to gain more insight (Alhammoud et al., 2010; De La Vara et al., 2015; Krijgsman and Meijer, 2008; Meijer, 2006; Simon and Meijer, 2015; Topper and Meijer, 2015). A special effort has been put into understanding how the Mediterranean gateway restriction influenced the Mediterranean environments and how the non-linear response of salinity to said restriction led to the MSC (Meijer, 2012).

In contrast, for the pre-MSC, continuous sedimentological and micropaleontological records exist all over the Mediterranean basin. High resolution micropaleontological (Bulian et al., 2021; Corbí et al., 2020b; Di Stefano et al., 2010; Hüsing et al., 2009; Kouwenhoven et al., 2006; Kouwenhoven et al., 2003b; Santarelli et al., 1998; Seidenkrantz et al., 2000; Sierro et al., 2003; Sprovieri et al., 1996a) and geochemical (Filippelli et al., 2003; Karakitsios et al., 2017a; Karakitsios et al., 2017b; Moissette et al., 2018; Nijenhuis et al., 1996; Schenau et al., 1999; Vasiliev et al., 2019; Vázquez et al., 2000) studies performed on Mediterranean locations, point to a drastic change in Mediterranean environments as early as 7.17 Ma ((Bulian et al., 2021), dating by astronomical turning (Hilgen et al., 1995; Lirer et al., 2019)), hereafter referred to as the 7.2 event. From this time onward, benthic foraminifers indicative of stressful conditions become dominant basin-wide and the stable carbon isotope records show a sharp drop towards lighter values (Bulian et al., 2022; Kouwenhoven et al., 2003b; Sprovieri et al., 1999) suggesting changes in bottom-water residence time. Contemporaneously, elemental and planktic foraminifer records of the western Basin start showing a cyclical pattern (Bulian et al., 2022; Bulian et al., 2021; Sierro et al., 2003), while in the eastern Basin the sapropel layers become a more regular feature in the sediments (Hüsing et al., 2009; Kontakiotis et al., 2022; Krijgsman et al., 1994; Seidenkrantz et al., 2000; Zachariasse et al., 2021) and show a cyclical pattern analogous to the faunal changes. The materialization of such cyclicity in the Mediterranean sedimentological record is assumed to be the result of astronomically driven changes in the freshwater budget that become more expressed as the basin isolates from the global ocean, rendering it increasingly sensitive to climate forcing (e.g. Bulian et al., 2021; Butiseacă et al., 2022; Sierro et al., 2003). The influence of restriction on the Mediterranean water properties has been previously studied with a high resolution model in (Topper and Meijer, 2015). However, long term and transient responses of salinity, overturning strength or salinity gradients have so far not been investigated. Consequently, there is a need to model the preconditioning phases of the MSC in more detail. In this work we present a box model study with the aim of testing whether

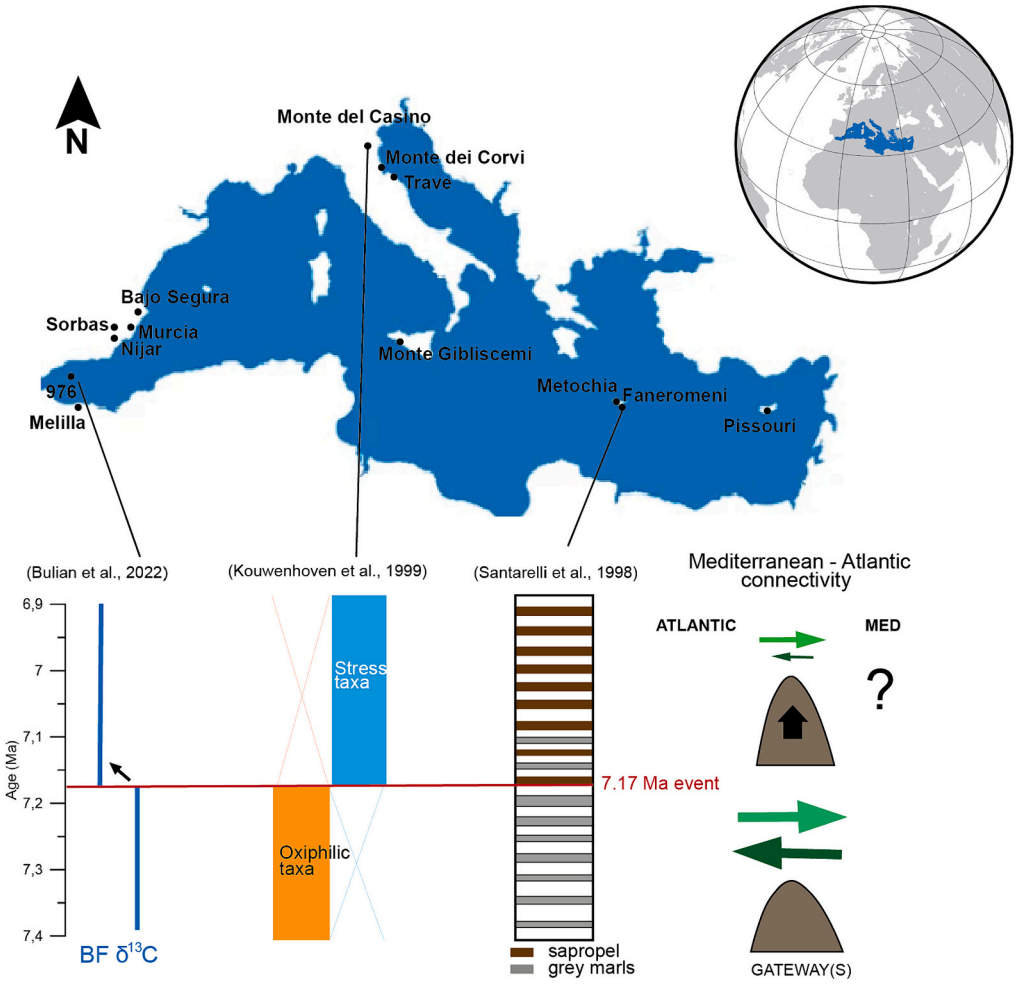

Fig. 1. Map in upper part shows various locations where the 7.17 Ma event has been identified, from (Bulian et al., 2022; Bulian et al., 2021; Corbí et al., 2020b; Di Stefano et al., 2010; Fortuin and Krijgsman, 2003; Hüsing et al., 2009; Kouwenhoven et al., 1999; Kouwenhoven et al., 2003b; Rouchy et al., 2003; Santarelli et al., 1998; Seidenkrantz et al., 2000). Below the map some examples of the different changes that affected the Mediterranean Basin after 7.17 Ma, from left to right: simplified trend of the benthic foraminifer δ13C record from West Alboran Basin ODP Site 976; schematic representation of the dominant benthic foraminifer taxa at Monte del Casino section; stratigraphic log of the Faneromeni section; schematic representation of the possible mechanism behind the 7.17 Ma event.

an early decrease in the connectivity between the Mediterranean Sea and the Atlantic Ocean could have been the first step in a process that eventually led to the MSC or whether a change in the freshwater budget could have been the sole driver for this event.

1.1. Oceanographic background

The Mediterranean Sea (Fig. 1) is a semi-enclosed sea that is, at present, connected to the Atlantic through the Strait of Gibraltar, a ~ 300 m deep and ~ 13 km wide channel (Bergamasco and Malanotte-Rizzoli, 2010). Shallow in comparison to the abyssal depth of the basin, the exchange through this channel has an influence on the circulation of the entire basin (Candela, 1991). The shallow inflow does not only compensate for the net water loss to the atmosphere but also for the loss of Mediterranean Outflow Water (MOW) that is formed by a deep outflow. The latter is flowing through the same strait but in the opposite direction making it a two-way exchange (Astraldi et al., 1999; Bryden and Kinder, 1991). Due to this limited exchange, the Mediterranean Sea acts as a sensitive recorder of changes in forcing, which makes its marine stratigraphic sequence an archive of the Earth climatic system (Rio et al., 2003). The dense and saline outflow has been traced back to the late Tortonian (7.51 to 7.35 Ma) (de Weger et al., 2020; De Weger et al., 2021) when the Strait of Gibraltar was most likely still closed and the Mediterranean Sea was connected with the Atlantic by the Betic and Rifian corridors (Benson et al., 1992; Santisteban and Taberner, 1983). This dense outflow may have had an influence on the Atlantic circulation, e.g. (Rogerson et al., 2012), and its presence implies the existence of a two-way exchange through at least one of the straits (De La Vara et al., 2015) as well as the existence of an overturning cell in the Mediterranean Sea (Waldman et al., 2018). Although the circulation of the Mediterranean Sea is much more complex, it can be summarized saying that winter cooling and increased evaporation lead to an unstable water column and consequently to convection events with deep water formation in some parts of the basin (Waldman et al., 2018).

The circulation is thus driven by density instabilities that are made possible by the net evaporative water loss creating a horizontal gradient in the sea surface salinity with values increasing with distance from the strait. The net loss of fresh water also creates a salinity difference between the Atlantic and the MOW, (Lacombe and Richez, 1982)(Fig. 2).

2. Methods

The influence of a closing strait on the dynamics of the Mediterranean Sea will be explored with a transient box model that represents the essential processes that dominate the circulation of the Mediterranean Sea. The way they are translated into the model as well as the metrics we will use to analyse the forcing and the results of said model will be explained in this section.

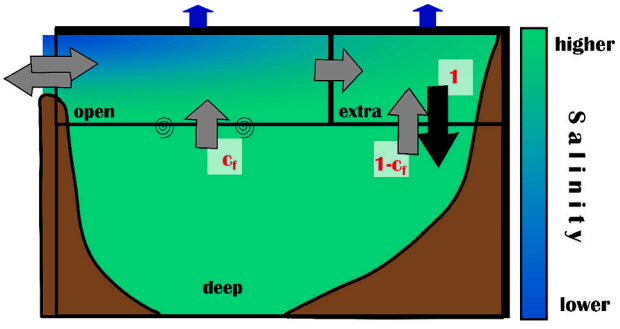

Fig. 2. Sketch of the box model with the boxes superimposed on a schematic depiction of the salinity gradients. The system is divided into three boxes with constant volumes (open, extra and deep) that interact with each other via fluxes (grey arrows) and mixing (spirals). The two upper boxes (open and extra) are subject to net evaporation (blue arrows), while the open box is also in exchange with the Atlantic (shown on the left). An overturning cell can form through (1) the downward resultant of the convective fluxes between extra and deep box, and (2) the return flux from deep to open box. The red labels give the size of the vertical fluxes, normalized to the flux from extra to deep.

2.1. The model

The model has been implemented in python and is based on previous box models set up to describe salinity gradients in the Mediterranean Sea during the Messinian (Ebner and Meijer, 2024; Simon and Meijer, 2017). As such it describes the Mediterranean Sea via three boxes (open, deep, extra, Fig. 2) with constant volumes that interact with each other and the Atlantic. Only the latter is treated as an unlimited reservoir with constant values. The open box is the one that is influenced by the Atlantic directly, the extra box represents the areas with the highest salinity and the deep box represents the deep-water masses. These boxes thus do not represent specific subbasins within the Mediterranean but together allow to represent the essence of the Mediterranean circulation, i.e. an overturning cell (between extra and deep box), a horizontal (between open and extra box) as well as a vertical (between open and deep box) salinity gradient and a two-way exchange with the Atlantic (between Atlantic and open box). The connection to the Atlantic will be represented by a single gateway which suffices because this study does not focus on absolute exchanges but on relative changes due to variation in connectivity.

Although in the oceans water density is influenced by three main factors: salinity, temperature, and pressure, in this model we will focus on salinity and use this property to express density differences.

Following the set-up in Fig. 2, the change in Salinity dS within one timestep dt in a volume V can be described by the water fluxes F between two boxes, the salinity they carry, as well as the flux of salt mass j_{mix} that occurs due to mixing along the horizontal interface between the open and the deep box. The latter is calculated following the common approach for diffusive processes (Dirksen and Meijer, 2020; Matthiesen and Haines, 2003; Tziperman and Speer, 1994) via the area A_{open} of the interface, a mixing length scale d_{mix} and a mixing parameter κ_{mix}.

$$j_{mix} = \kappa_{mix} \cdot \frac{A_{open}}{d_{mix}} \cdot \left(S_{open} - S_{deep}\right) \tag{1}$$

Where S_{open} and S_{deep} are the salinity in the open and deep box, respectively. The water flux that drives the vertical circulation originates in the extra box. Whenever there is an unstable stratification with $S_{extra} > S_{deep}$, convection is taken to occur which is represented by a downward and an upward flux. Complete convection would entail these fluxes to be equal. However, consistent with observations of the present-day Mediterranean Sea (Waldman et al., 2018), the model allows for a net downwards flux, which means that the upwards flux is smaller than the one downwards. The flux from the extra to the deep box is derived similar to the mixing from the interface between the extra and the deep box, using A_{extra}, a scaling parameter κ_{conv} and the relative salinity difference to reflect reduced buoyancy of the sinking flux (Ebner and Meijer, 2024):

$$F_{extra \to deep} = k_{conv} \cdot A_{extra} \cdot \frac{max\left(0 S_{extra} - S_{deep}\right)}{S_{deep}} \tag{2}$$

The upwards flux then, is described by

$$F_{deep \to extra} = \left(1 - c_f\right) \cdot F_{extra \to deep} \tag{3}$$

where the coefficient c_f with $(0 < c_f < 1)$ determines the extent to which convection is incomplete. The overturning cell is closed by an upward flux from the deep to the open box, equal in size to the resultant of the two convective fluxes.

The downwards component of the convection is the only influx into the deep box, it is also the main influence on the residence time of water in it, because the influence of mixing is relatively small and can be

neglected.

$$T_{res} = \frac{V_{deep}}{F_{extra \rightarrow deep}} \tag{4}$$

The only other flux of water that is defined by a salinity difference is the outflow Q_{out} from the open box to the Atlantic. Its strength is based on the concept of hydraulic control as presented in (Meijer, 2021; Meijer, 2006) and driven by the salinity difference between the open box and the Atlantic. The proportionality between this difference and the outflow is set by g, where smaller values of g describe a more restricted connection. The unit of g is with $(m^3/s)/\sqrt{kg/m^3}$ quite bulky and will be omitted from here onwards.

$$Q_{out} = g^* \sqrt{S_{open} - S_{Atl}} \tag{5}$$

The inflow through the gateway is not only replacing the outflow, but also the freshwater budget fwb that is expressed as the net evaporation rate e that is acting on the surface A

$$Q_{in} = Q_{out} - fwb_{tot} = g^* \sqrt{S_{open} - A_{Atl}} + e \cdot A_{tot} \tag{6}$$

The outflow, represented by Q_{out}, thus originates in the open box, but is–due to the overturning cell–strongly influenced by the water of the deep box. Complementing $F_{extra-deep}$ and Q_{out}, the other fluxes result from the conservation of water mass. The complete expressions that describe the evolution of salinity for each of the three boxes are:

$$V_{open}\frac{dS_{open}}{dtk} = Q_{in}S_{Atl} + c_f F_{extra \rightarrow deep} S_{deep} - \left(Q_{out} + c_f F_{extra \rightarrow deep} + eA_{extra}\right) S_{open} - j_{mix} \tag{7}$$

$$V_{extra}\frac{dS_{extra}}{dt} = \left(c_f F_{extra \rightarrow deep} + eA_{open}\right) S_{open} - F_{extra \rightarrow deep} S_{extra} + \left(1 - c_f\right) \cdot F_{extra \rightarrow deep} S_{deep} \tag{8}$$

$$V_{deep}\frac{dS_{deep}}{dt} = -\underbrace{c_f F_{extra \rightarrow deep} S_{deep}}_{to open box} - \underbrace{\left(1 - c_f\right) F_{extra \rightarrow deep} S_{deep}}_{to extra box} + F_{extra \rightarrow deep} S_{extra} + j_{mix} \tag{9}$$

2.2. Metric for analysis

The model always starts at Atlantic salinity as a natural initial condition and thus needs time to stabilise and adjust itself to the given restriction (g) and sinusoidal forcing (e). A run ends with a dynamic stable state that repeats with each precessional cycle (Fig. 3). Since the duration of the spin-up phase depends on the restriction applied to the model, each run is only analysed after 5 cycles. This is enough time for even the most restricted scenarios to not be influenced by the initial values anymore.

To compare the resulting states for a range of strait restrictions, three different descriptors were chosen (Fig. 3). These are the amplitude a of the output, the average value over one precessional cycle b (baseline from which the amplitude is measured) and the ratio between these two. This metric is applied to all salinities, salinity differences and fluxes. By using these three descriptors, we can do two things: a) find the best sinusoidal representation for the reconstructed freshwater budget of the Mediterranean (Fig. 4) to use as forcing e for the model and b) compare a multitude of different set-ups to describe trends and identify possible configurations for before and after the event.

2.3. Numeric values

Although simple and minimalistic, this model still contains several parameters (see Table 1) of which most only have an influence on the absolute values of the output, but not on the general behaviour of the model (Ebner and Meijer, 2024).

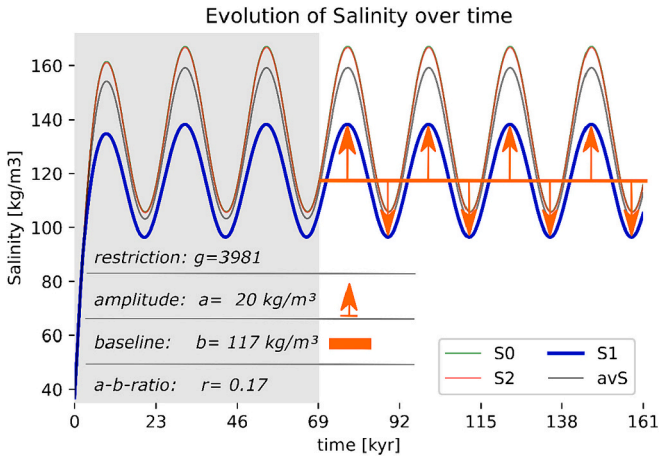

Fig. 3. Example of one model run with indication of the descriptors. Using the salinity of the upper box (S1, blue sinusoid) as an example the definition of the chosen descriptors a and b are shown for a model run with $g \approx 4000 \rightarrow log(g) \approx 3$. After the model had time to reach a dynamic steady state, the output varies with a constant amplitude around the baseline as response to the changes in the freshwater budget. The strait restriction is kept constant.

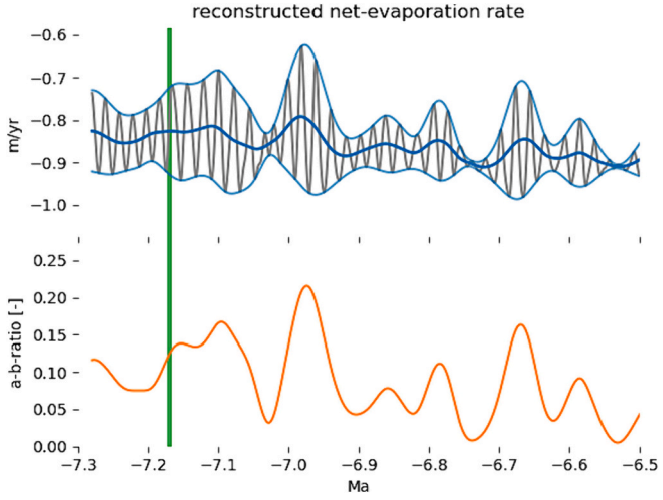

Fig. 4. Reconstructed net-evaporation rate (grey), based on (Simon et al., 2017), with baseline (dark blue) as well as the upper and lower envelope (light blue). The lower panel shows how the a-b-ratio changes over time. The green vertical line marks the 7.17 Ma event. While the baseline of the net-evaporation does not change much around that time, the amplitude does increase.

The total volume V of the model and its surface area A represent the water volume and surface area of the late Messinian Mediterranean Sea (Meijer et al., 2004). This translates to a cuboid with a depth D of ca 1.5 km. This total depth is distributed among the two layers of the model. The upper layer (open and extra box), which represents the surface and intermediate water masses has a thickness of 500 m. This makes the deep box, with a thickness of 1000 m, the largest water mass in the model.

Since the upper layer consists of two boxes, open and extra, the surface area A needs to be distributed among them. In this model the open box takes up 80% of the total surface area A, leaving 20% for the extra box. The choice of this distribution does influence the absolute values, but not the behaviour of the model we want to test here.

The vertical exchange in the model also has two components. The first being mixing and the second convection as expressed by the $F_{trigger}$ and its response fluxes. The mixing coefficient $\kappa_{mix} = 5 \cdot 10^{-4} m^2/s$ is based on the background mixing as it has been used in previous model

Table 1
Parameters and how they are used in the model.

	Value in model	Description
A	$A = 2.5{\cdot}10^{12}\ m^2$ (Meijer et al., 2004) $A_{open} = 0.8{\cdot}A_{tot}$ $A_{extra} = 0.2{\cdot}A_{tot}$ $A_{deep} = A_{tot}$	Surface area of the Mediterranean Sea and areas that describe the boxes (Meijer et al., 2004)
D	$D = 1.5km$ $D_{open} = 500m$ $D_{extra} = 500m$ $D_{deep} = 1000m$	Depth of the boxes
V	$V = 3.8{\cdot}10^{15}m^3$ $V_{extra} = A_{extra}{\cdot}500\ m$ $V_{open} = A_{open}{\cdot}500\ m$ $V_{deep} = A_{tot}{\cdot}1000\ m$	Volumes of the boxes used in the model (Meijer et al., 2004)
e	$(0.86 \pm 0.095)m/yr$ (first part of results) $(0.86 \pm 0.065)m/yr$ (before event) $(0.86 \pm 0.11)m/yr$ m/yr (after event)	Net-evaporation, used as forcing in the model (Simon et al., 2017)
fwb	$-\ [5.8, 7.4]{\cdot}10^4 m^3/s$	Range of freshwater budget of the basin between 7.28 Ma and 7.1 Ma. This expresses the same information as e, but in $[m^3 s^{-1}]$. The fwb is negative for a loss of freshwater due to evaporation (Simon et al., 2017)
S	$S_A = 36kg/m^3$ $S_{lim} = 50kg/m^3$ $S_{extra}, S_{open}, S_{deep}$	Salinity of the inflow from the Atlantic, maximum salinity after the 7.2 event and the three model boxes
T	2000 *yr*	Period of precessional cycle in model
dt	1 yr	Timestep of the model
g	$g = [10^3, 10^7]m^3/s\left(\sqrt{kg\,m^{-3}}\right)^{-1}$ $g_{open-marine} = 10^6\ m^3/s\left(\sqrt{kg\,m^{-3}}\right)^{-1}$ $g_{restricted} = 10^5\ m^3/s\left(\sqrt{kg\,m^{-3}}\right)^{-1}$	Range of the scaling parameter for the exchange between the Mediterranean Sea and the Atlantic, restriction parameter
c_f	0.9	Fraction of dense water that is forming the net-downwards flux
Q	$[m^3/s]$	Exchange between the Mediterranean Sea and the Atlantic (fwb <0)
F_{ab}	$[m^3/s]$	Water flux from box a to box b
j_{mix}	$[kg/s]$	Salt flux due to mixing
κ_{conv}	$8{\cdot}10^{-4}m^3/s$	Scaling parameter for convection
d_{mix}	750 *m*	Mixing length
κ_{mix}	$5{\cdot}10^{-4}m^2/s$	Mixing parameter

studies (Dirksen and Meijer, 2020). The coefficient $\kappa_{conv} = 8{\cdot}10^{-4}m^3/s$ that scales the strength of $F_{trigger}$ has been chosen in a way that said flux has a strength comparable to today (Waldman et al., 2018).

The choice of $c_f = 0.9$ also has a small influence on the absolute values (salinity, salinity differences and fluxes), but it does not influence the behaviour of the model (Ebner and Meijer, 2024), which is what we are focussing on in this study. Same applies to the salinity S_A of the inflow.

The degree of restriction, however, has a large influence on the response of the model to its forcing. The model is thus run with 150 different degrees of restriction ranging from 10^7 to 10^3. To model the reaction of the system to a connection that gets more restricted over time, starting at $g_{open-marine}$ and ending at $g_{restricted}$. The timespan of this restriction is chosen arbitrarily as we know too little about potential restriction processes and the connection(s) itself to make an educated guess. The upper limit, $g_{open-marine}$, is defined by the open marine conditions of the Mediterranean Sea before the 7.2 event (Blanc-Valleron et al., 2002; Bulian et al., 2022; Kouwenhoven et al., 2003a; Seidenkrantz et al., 2000). The lower limit, $g_{restricted}$ that leads to a basin with higher salinity is determined from the steady state solutions in the first part of the results and is defined by the maximum salinity, $S_{lim} = 50kg/m^3$ (aprox. 50‰; in the context of this study the difference between kg/m^3 (model) and ‰ (data) is negligible). This is based on high abundances in planktonic foraminifer *Orbulina universa,* (Bulian et al., 2021; Morigi et al., 2007; Sierro et al., 2003) and experiments that indicate that this species survives in salinities up to $46kg/m^3$ ($\approx$ 46‰) (Bijma et al., 1990). In addition, Kontakiotis et al. (2022) obtained a TEX_{96}^{H} based Sea Surface salinity record for an Eastern Mediterranean section (Agios Myron, Heraklion Basin) from which it can be concluded that after 7.2 Ma, and especially at 6.9 Ma, salinities of around 45 ‰ were reached in the basin.

The net evaporation *e*, defined by average and amplitude (Fig. 3) is a forcing parameter that is relevant for the scope of this paper. The net evaporation is determined from reconstructions of the Mediterranean freshwater cycle by (Simon et al., 2017) (Fig. 4). This reconstruction is based on 31 coupled climate simulations with different orbital configurations in combination with a regression model to compute the freshwater budget between 7.25 Ma and 5.33 Ma from the orbital curves (Laskar et al., 2004). For the model, this reconstruction is simplified to a net evaporation rate *e* that oscillates around 0.86 m/yr ((Simon et al., 2017), shown in Fig. 4) with a period of $T = 20\ kyr$ to approximate one precessional cycle. During this cycle *e* varies sinusoidally with an amplitude that is described in percent of the baseline (*a*-b ratio; Fig. 4, lower panel). For the first part of the results *e* varies between 0.765m/yr and 0.955m/yr resulting in an amplitude of 11% of the baseline, for the second part *e* switches from varying between 0.796m/yr and 0.925m/yr to 0.731m/yr and 0.989m/yr, which results in an amplitude of 7.5% and 15%, respectively.

3. Results and analysis

The results are represented in two parts. In the first part we will analyse the response of the model to different levels of strait restriction (*g*) using the metric presented above. Those different steady states are then compared to the situation before and after the event (Fig. 5). In the second part, this information is used to test how the system behaves when it becomes gradually more restricted over a certain interval of time (Fig. 6).

3.1. Steady states

The model is forced with a sinusoidal fwb with a constant period of 20 *kyr*, a baseline of $0.86m/yr$ and an amplitude of 11%. While the strait restriction is kept constant within a given run, a series of runs has been conducted covering a broad range of degrees of strait restriction, $10^3 \leq g \leq 10^7$. Hence, the results in Fig. 5 provide insight in how the response of the system to a given forcing changes in dependency of strait restriction. This is then used to define the lower and the upper estimate for the state of the system before and after the 7.2 Ma event, respectively. As described in the **Error! Reference source not found.**, the graphs do not show the transition from one restricted state to the other but rather a sequence of dynamic steady states for a constant restriction in sinusoidal fwb as forcing.

The baseline of the average salinity of the basin (Fig. 5a) behaves as described in previous studies (Meijer, 2012; Meijer et al., 2004; Topper and Meijer, 2015). It increases in response to lower values of *g* and does so in a non-linear way. Its amplitude also increases, which implies an increase of the range of average salinity that the basin attains within a precessional cycle. This is indicated by the broadening of the blue band and also shows in the increase of the a-b-ratio. The latter indicates that the amplitude is increasing even faster than the baseline (average over one precessional cycle). This means that the same amplitude in the sinusoidal freshwater forcing creates a larger absolute as well as relative amplitude in the salinity for a more restricted basin. This increase in

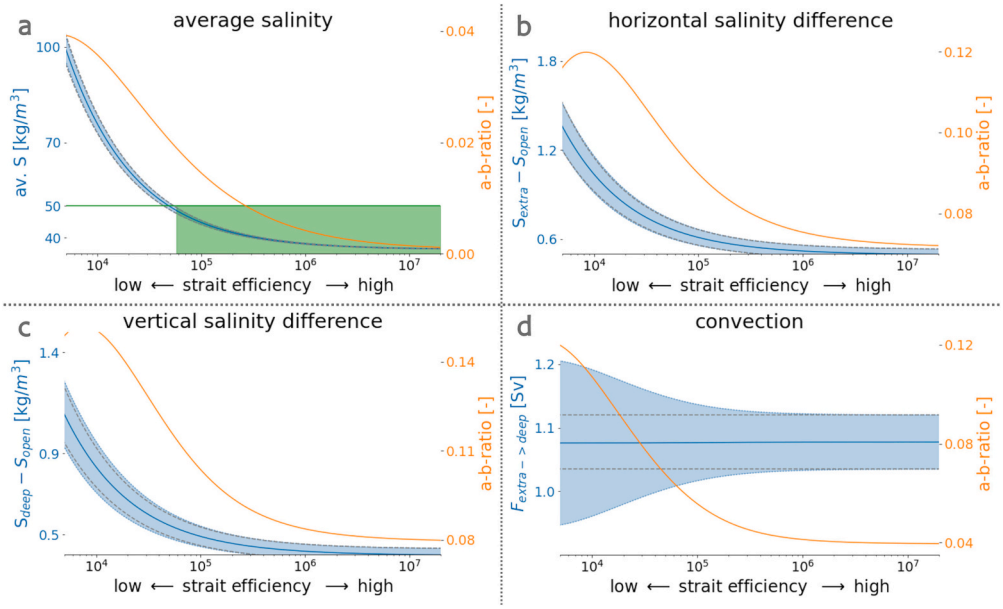

Fig. 5. Dependence on strait efficiency (g, x-axis). The blue line (left y-axis) shows the mean of the parameter over one precession cycle while the blue shaded area indicates the whole range of values for the same period. The dashed grey lines indicate the values that would result from a model that is forced with a constant net evaporation rate that corresponds to the minimum (lower) and maximum (upper) of its sinusoidal counterpart. The scale for the a-b-ratio (orange) is on the right-hand side y-axis. (a) Mean salinity of Mediterranean basin. Shows a clear non-linear response of the basin to a change in the strait restriction. The green shading indicates the range of values for g that correspond to a pre-event salinity and thus indicates the lower limit for g. (b) Horizontal salinity difference defined as the salinity difference between the open box and the extra box. A positive value represents an increase in salinity with distance from the strait. (c) The salinity difference between the open box and the deep box (box 2) is a measure for stratification in the model (d) The convection between the extra and deep box is represented by the strength of the downwards flux (not the net flux) and can be considered to describe the ventilation of the Mediterranean deep waters.

sensitivity thus shows that a change in the river inflow rate or the evaporation has a stronger influence on the system when the basin is more restricted. However, the a-b-ratio reaches a peak for $g \approx 10^4$. Baseline and amplitude are still increasing after this peak, but the increase of the amplitude slows. The theoretical maximum of the salinity increases for smaller values of g, and so does the time the model needs to reach this value. Thus, this peak would occur for lower values of g if the period was larger than $T = 20\ kyr$.

Comparable trends can also be seen for the horizontal salinity gradient (Fig. 5b) and the stratification (Fig. 5c). The more restricted the basin is, the larger the baseline and amplitude become. The convection (Fig. 5d), however, only shows an increase in sensitivity, while the baseline stays constant. This means that the absolute extremes within one precessional cycle are increasing, while the strength of the forcing, amplitude and baseline of e, remains constant.

3.2. Transition over time

To test the influence that a gradual change of the strait efficiency would have on the system, we reduce g within 6 precessional cycles (120 kyr) from a higher to a lower value. The higher restriction parameter, $g_{open-marine} = 10^6$, is representing the almost open marine conditions before the event and the smaller one the more restricted system after the event. The latter is read from Fig. 5a with the assumption that the sea surface salinity (SSS) and thus the average salinity increased without exceeding $S_{lim} = 50 kg/m^3$. With this we get a lower limit for the strait restriction after the event with $g \approx 5{\cdot}10^4$ (Fig. 5a, green line). Considering this information, we choose a restriction of $g_{restricted} = 10^5$ for the following experiments. This will result in a lower average salinity but will otherwise not change the behaviour of the model. To explore the influence that a change over time has on the salinities and convection, and thus the transition of the model from one state into the other we will compare three scenarios. In the first the connectivity of the strait is decreased from $g_{open-marine} = 10^6$ to $g_{restricted} = 10^5$ and kept constant before and after this transition (Fig. 6). The model (Fig. 2) is again forced by a sinusoidal freshwater budget, of which the amplitude is first kept constant at 11% (Fig. 6a). In the second scenario the amplitude is doubled from 7.5% to 15% (Fig. 6b) to capture the changes in the forcing that seem to have occurred around 7.2 Ma (Fig. 4, second panel). A third scenario shows how the system responds to the same change in freshwater budget, but without a change in restriction (Fig. 6c). The response of the system over time shows that a gradual change of one parameter, as here the restriction g, can cause a non-linear response of the system (Fig. 6a), which is especially visible in the salinities. Although there is an immediate response in terms of slight increases when the connectivity begins to decrease, >60% of the salinity increase occurs in the last half of the last cycle of the transition from less to more restricted. When the change in restriction stops, the system balances itself with a brief episode of increased convection, overshooting (Fig. 6a and 6b). Shortly after, the system reaches its new stable state with a higher average salinity as well as a larger amplitude throughout the cycle.

There are only small differences between the scenarios when looking at the convection. Neither of the changes has a notable influence on the baseline as it is barely influenced by either the change in restriction or the change of the fwb. All three scenarios however produce a change in the amplitude. The first one due to an increase in sensitivity (Fig. 6a), the third due to a larger amplitude in the forcing (fwb) (Fig. 6c), and the second due to a combination of those two effects (Fig. 6b).

4. Discussion

4.1. Limitations of the model set-up

As described in previous sections, this model is set up to discuss trends rather than absolute values. As such the model is a simplified representation of the Mediterranean as one basin. The implementation focusses on the three elements that are of interest, salinity, freshwater budget, and restriction. While adding additional boxes or parameters,

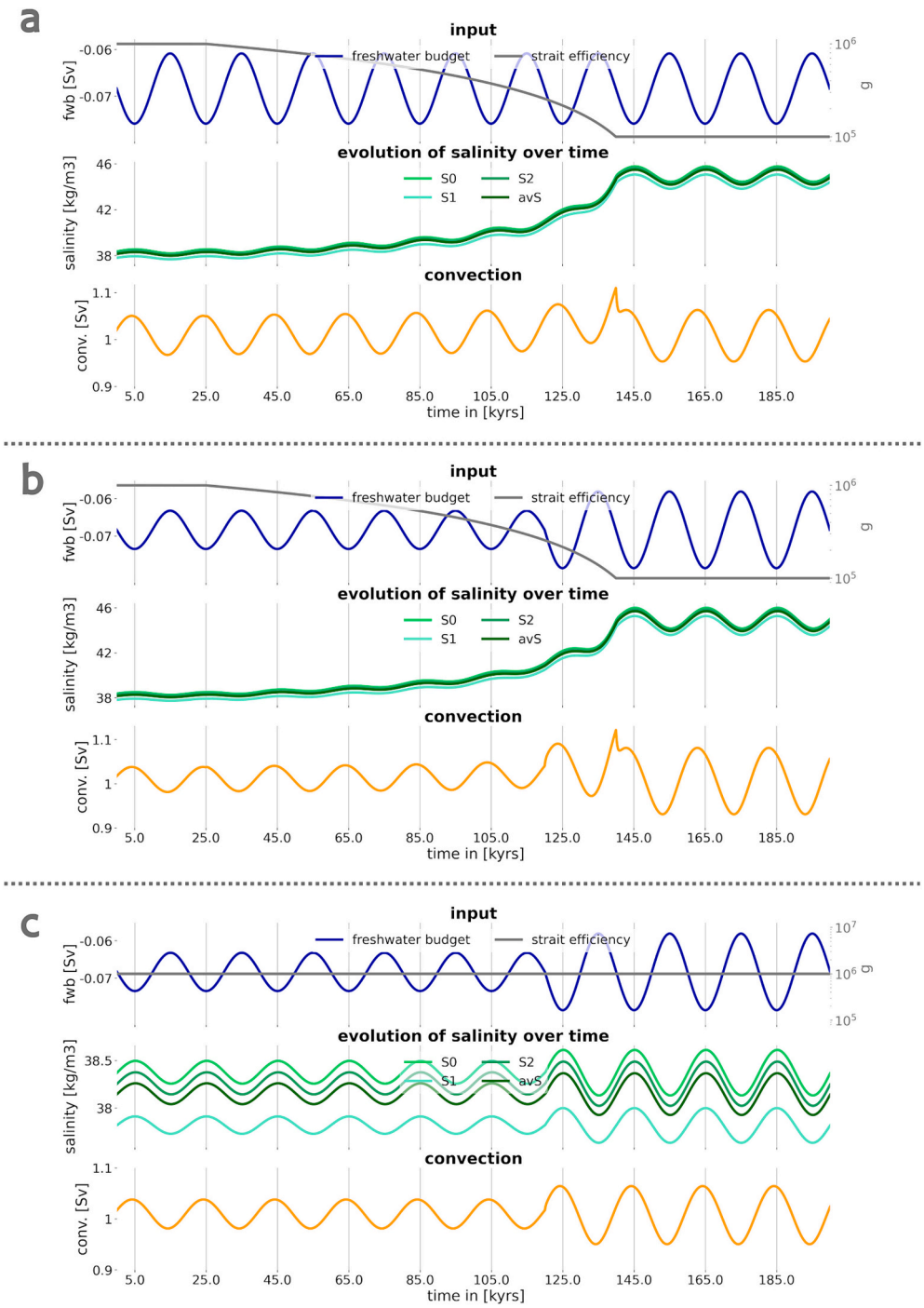

Fig. 6. Three scenarios with time-dependent forcing. The top panel of each scenario displays the change in restriction (grey, right y-axis, logarithmic), that is applied and the freshwater budget (blue, left y-axis, linear) that forces the model. The response of the system to this input is shown in the two following panels in terms of salinities (shades of green, middle panel), salinity differences and convection (orange, bottom panel). (a) Response to a gradual decrease in strait efficiency; Here a linear change in the parameter g is applied while the freshwater budget only changes throughout one cycle. (b) Response to a combined change in restriction and fresh water budget; c) Response to a sudden change in the freshwater budget with constant restriction.

such as temperature, would make the model more realistic this would also increase complexity and uncertainty.

4.2. Explanation of the model results

Our model results can be used to assess two kinds of effects that a change in restriction has on this semi-enclosed basin. Not only could we compare the steady states of the system for different degrees of restriction, but we also modelled the transition from one state to the other.

The most obvious change is the increase in salinity as a response to an increase in restriction. This is easily explained by the salt mass balance in the basin. For a stable state the influx of salt mass is equal to the outflux, which can be expressed by the Knudsen theorem (Knudsen, 1900).

$$S_{atl}{}^{*}Q_{in} = S_{Med}{}^{*}Q_{out} \text{ with } Q_{in} = Q_{out} - fwb \text{ and } fwb < 0 \quad (10)$$

The salinity of the Mediterranean Sea is then dependent on the constant salinity of the Atlantic Ocean and the ratio between freshwater

budget and outflow, which is scaled by the restriction parameter g.

$$S_{Med} = S_{Atl}\left(1 + \frac{|fwb|}{Q_{out}}\right) \quad (11)$$

The smaller the freshwater budget is compared to the outflux, the closer the basin salinity is to the inflow salinity: which means that the strait exchange dominates the behaviour, and basin-water properties stay close to those of the ocean. When the basin becomes more restricted (low values of *g*), however, the outflux becomes smaller and the ratio $|fwb|/Q_{out}$ increases, leading to a higher salinity in the basin. The same ratio also influences the sensitivity of the basin. The smaller the outflux through the strait, compared to the net freshwater flux to the atmosphere, the more the basin salinity is influenced by fluctuations and rate of change in freshwater flux.

Other changes, like in stratification, are a result of the increasing salinity difference between inflow and the basin salinities. While the inflowing waters from the Atlantic, which are mainly affecting the open box, do not increase in salinity, the salinity of the extra box does. This increase in salinity difference is keeping the open box at a lower salinity than the other boxes. It is, so to say, diluted by Atlantic waters. This results in both a stronger stratification ($dS_{deep-open}$) and stronger horizontal salinity gradient ($dS_{extra-open}$). In contrast, the baseline of the relative salinity difference between the extra and the deep box $dS_{extra-deep}/S_{deep}$, and thus the baseline of the convection (i.e., the temporal average of the sinking flux from the extra to the deep box) stays stable. The increase in amplitude is a reaction to the rate of change in the forcing and vanishes for longer cycles. This is in agreement with previous model studies showing that the strength of the convection cell does not change when the basin gets more restricted (Topper and Meijer, 2014).

It is important to point out that the residence time of the basin increases when it becomes more restricted, since the flux from the Mediterranean Sea to the Atlantic Q_{out}, decreases. The change in the residence time of the deep box is more complex. Averaged over one precessional cycle it does not change since the baseline of the convection does not change, but due to the increased sensitivity (caused by the change in restriction) and the larger amplitude of the fwb its extrema change. For the dry phase the residence of the deep box decreases (stronger convection) while it increases for the wet phase (insolation maxima, weaker convection).

With the gradual change in restriction, we can reproduce a non-linear change in baseline and amplitude of the salinities (Fig. 6a). This non-linear behaviour also occurs when Q_{out} depends linearly on the salinity difference between the Atlantic and the open box. To provoke a sudden change in the model salinity and circulation, this change in restriction must be large enough and sufficiently fast. If the change is too small, then there is no noticeable difference between the initial state and the end state. If the period during which this restriction occurs is too long, then the non-linear response of the system is not leading to noticeable change from one cycle to the other and would then no longer be perceived as an abrupt change. Only a sufficiently high rate of change can provoke a response that can be described as sudden. For the change from open marine to restricted (g reduced by one order of magnitude) the timescale considered in this paper (6 precessional cycles, 120 *kyr*) is sufficient to show this effect. The disruption in the system also causes an overshoot in the convection when the model relaxes into the new state. For shorter timespans both effects would become more pronounced.

4.3. Implications for the geological question

One of the aspects that characterise the 7.2 Ma event is the sudden change displayed by the salinity proxies. Even though several micropaleontological and geochemical field data demonstrate analogous changes, a reliable independent proxy for salinity is unfortunately still missing and several recent attempts of producing one yielded contrasting results. Sea surface salinities (SSS) obtained from the combination of planktonic foraminiferal isotopes ($\delta^{18}O$ *Globigerinoides obliquus*) and TEX86-SSTs from Potamida section in western Crete yielded a salinity increase from 36 to 38 ‰ to 46–47 ‰ visible already from the uppermost Tortonian (Besiou et al., 2021). Similar results were obtained for the Agios Myron section (Kontakiotis et al., 2022). On the other hand, SSS estimates for Faneromeni section located in the same island and estimated through $\delta^{18}O$ measurements from the same planktic foraminifer species, show an opposite behaviour and a SSS decrease from ~40 ‰ to 38–36 ‰ after 7.2 Ma (Kontakiotis et al., 2019). Consequently, salinity changes are still being tentatively deduced mainly from the planktic and benthic foraminifer associations and changes in the $\delta^{18}O$ record. Field data from several Mediterranean locations (Bulian et al., 2021; Kouwenhoven et al., 2006; Morigi, 2009; Morigi et al., 2001; Morigi et al., 2007; Sierro et al., 2003; Sprovieri et al., 1996a; Sprovieri et al., 1996b), show, starting at 7.17 Ma, high abundances of the planktic foraminifer *Orbulina universa,* known to tolerate hypersaline conditions. In laboratory cultures, this species has been found living between a salinity of 23 and 46 ‰ (Bijma et al., 1990), meaning that the Mediterranean salinity after 7.17 Ma may have increased but remained below ~46 ‰. At the same time an increasing abundance of stress-resistant taxa like bolivinids, buliminids and several *Uvigerina* species (Di Stefano et al., 2010; Drinia et al., 2007; Kouwenhoven et al., 2006; Violanti et al., 2013) suggest the beginning of stressful environmental conditions, possibly including increased salinity and reduced oxygen levels. Finally, the increase in $\delta^{18}O$ that characterizes the 7.17 Ma event (Blanc-Valleron et al., 2002; Kouwenhoven et al., 2003b; Seidenkrantz et al., 2000; Sprovieri et al., 1996a) could also suggest a rise in salinity (e.g. Conroy et al., 2017), but it can also be related with the contemporaneous Late Miocene Global Cooling (Herbert et al., 2016; Holbourn et al., 2018). Even though it is difficult to discern which signal, local or global is dominant, a recent study (Bulian et al., 2022) showed how in a restricted basin like the Mediterranean local changes are predominant and therefore $\delta^{18}O$ changes could be attributed to a salinity increase. Our model analysis shows that any increase in salinity cannot be explained by the change that occurred around 7.2 Ma in the freshwater budget, which would only influence the extrema, but not the average salinity over time since the baseline of the freshwater budget presumably did not change around the time of the event (Fig. 4). A more restricted connection to the Atlantic however could explain the increased stress of the system. The model results imply that a gradual change in said restriction could also explain the sudden nature of the expression in the proxy record, because of the inherent non-linearity of the system. In other words, the cause is already under way before we can see its effect expressed in the sediment. It also seems likely that the restricting event happened on a timescale of 120 kyr or less, since the changes in the proxy records described in (Bulian et al., 2022) appear to happen within one cycle. It, however, seems unlikely that the restricting process happened within much less time than this. This would increase the overshooting response of the convection and thus create well-ventilated deep waters, which would contradict the presence of the sapropel in the Faneromeni sections (Hilgen et al., 1995; Krijgsman et al., 1994; Santarelli et al., 1998) that formed in the wake of this event.

The second change that affected the Mediterranean after the 7.17 Ma gateway restriction is the increased sensitivity of the basin to climate forcing, as evidenced by field and core data. The marked cyclical pattern that appears after 7.17 Ma in Western Mediterranean locations like West Alboran Basin ODP Site 976 (Bulian et al., 2021) or Sorbas Basin Lower Abad Member (Sierro et al., 2003) has been interpreted as the response of the restricting Mediterranean to astronomical forcing. The contemporaneous increase in precession amplitude (Fig. 6b) has been considered as an additional factor amplifying the climate signal (Krijgsman et al., 2000) that the model analysis lends support to this notion, but also shows that a restriction would increase the sensitivity of the basin and thus enhance the influence of the change in climate signal (Fig. 5a-dc) as

well as an increase in water column stratification (Fig. 6c). In Alboran Basin Site 976, at 7.17 Ma, the first appearance of subtropical *Globigerinoides* spp. is considered to be indicative of a more stratified water column during the phases of maximum summer insolation that result in higher sea surface temperatures and the growth of subtropical species (Bulian et al., 2021). A combination of this increased sensitivity and stratification could also explain the sapropel formation, that becomes more frequent in the Eastern Mediterranean which is indicative of stagnation at the bottom during phases of summer insolation maxima. The summer insolation maximum also refers to the wet phase of the precessional cycle where high freshwater influx would prevent deep water formation and ventilation at the bottom (Rohling et al., 2015). Our model shows that a more restricted basin would react more sensitive to such an influx of freshwater which would increase the chances for weak convection and thus anoxia in the deep. This effect would again be enhanced by a larger variation in the fwb after the event (Simon et al., 2017). This combination of increased sensitivity and lower net evaporation rates during the wet phase would lead to more extreme situations that could lead to anoxic conditions due to weaker convection than before the event.

The model presented here thus supports the hypothesis that the Mediterranean-Atlantic gateway restriction resulted in an amplification of the astronomically driven cyclicity that was additionally boosted by the simultaneous precession amplitude increase resulting in the sharp shift in the record (Fig. 6).

The third aspect to consider is that several studies suggest that starting from 7.17 Ma, the deep-water residence time increased as a consequence of the gateway restriction and diminished water exchange between the Mediterranean and Atlantic (Bulian et al., 2021; Corbí et al., 2020a; Hüsing et al., 2010; Kouwenhoven et al., 2006). This has been inferred mainly from benthic $\delta^{13}C$curves for both the Western and Eastern Mediterranean (Bulian et al., 2022; Seidenkrantz et al., 2000). The $\delta^{13}C$ can be used as an indirect indicator of water residence time because the values get progressively lower through time by the addition of ^{13}C poor CO_2 derived from the oxidation of organic matter that is supplied during sedimentation (Blanc and Duplessy, 1982). From 7.17 Ma multiple Central and Eastern Mediterranean sites (e.g. Monte del Casino: (Kouwenhoven et al., 2003a; Krijgsman et al., 1997), Monte Gibliscemi: (Blanc-Valleron et al., 2002; Kouwenhoven et al., 2003a; Sprovieri et al., 1999; Sprovieri et al., 1996b) and Metochia sections: (Seidenkrantz et al., 2000)) show a sharp drop in $\delta^{13}C$ values of benthic foraminifers implying an increase in deep-water residence time. For the Western Mediterranean, the only available record of deep water masses during the late Tortonian, Site 976 located in the West Alboran Sea (Bulian et al., 2022), points to a ~ 1‰ decrease in the benthic $\delta^{13}C$.

In the model, the residence time of the whole basin increases as a result a more restricted connection with the Atlantic. The model, however, does not show a change in the average residence time of the deep basin, where residence time is set by the rate of convection. For the deep box, a more restricted connection results in increased sensitivity to the climatic forcing, i.e., larger changes in convection and thus a larger variation of residence time, while the average remains unchanged. This seems to contradict the observation that the drop in $\delta^{13}C$ occurs in the benthic but not in the planktic foraminifera, at least in correspondence with the 7.2 event. A shift in δ13C occurs only from 6.74 Ma in the Eastern Mediterranean site of Metochia (Zachariasse and Lourens, 2022) and Agios Myron (Zachariasse et al., 2021). It may imply that the model is flawed or incomplete in that it must include other aspects affecting the carbon isotopic composition than circulation. It could also be that the data are somehow biased towards the wet phase and not representative of the full precessional cycle, not representative of the residence time of the deep basin solely or reflecting a change in assemblage rather than circulation.

5. Conclusions

A first-order model for the overturning of the Mediterranean Sea offers physics-based support for the notion that sudden changes at 7.17 Ma that can be seen both in sediment cores and land-based sections from different parts of Mediterranean could have been caused by an increasing restriction of the Mediterranean-Atlantic gateway(s) and would have been amplified by changes in the freshwater budget. With this study we can confirm that the salinity increase, higher likelihood of sapropel deposition, larger salinity gradients (vertically and laterally) as well as the sudden nature of those changes could be explained by a restriction event that ended at 7.17 Ma. The effects of restriction are amplified by a change in atmospheric forcing that likely occurred around that time.

Additionally, the model analysis provides insight into the role of mean net evaporation versus that of its periodic variability and changes in amplitude. It also shows that an increased variation within one proxy during a precessional cycle does not necessarily refer to an increased variability of the climate forcing but can also be expression of an increased restriction of the basin. A gradual change in restriction can cause a non-linear response in the basin, when this happens on a short enough timescale then this response might seem abrupt. The shorter the timescale however, the more pronounced the peak in convection becomes that is needed to bring the system to its new balance. Our results also open the question if there might be aspects that have been missed in the interpretation of the proxy data. As such our model analysis supports the notion that the 7.17 Ma event is the first sign of the catastrophic change that led to the Messinian Salinity Crisis.

Funding information

This research is carried out under the SALTGIANT ETN, a European project funded by the European Union's Horizon 2020 research and innovation programme under the Marie Skłodowska-Curie grant agreement number 765256. SaltGiant: www.saltgiant-etn.com

CRediT authorship contribution statement

Ronja M. Ebner: Conceptualization, Methodology, Software, Validation, Visualization, Writing – original draft. **Francesca Bulian:** Conceptualization, Formal analysis, Validation, Visualization, Writing – original draft. **Francisco J. Sierro:** Supervision, Writing – review & editing. **Tanja J. Kouwenhoven:** Writing – review & editing. **Paul Th. Meijer:** Conceptualization, Supervision, Writing – review & editing.

Declaration of competing interest

The authors declare the following financial interests/personal relationships which may be considered as potential competing interests.

This research is carried out under the SALTGIANT ETN, a European project funded by the European Union's Horizon 2020 research and innovation programme under the Marie Skłodowska-Curie grant agreement number 765256. SaltGiant.

Data availability

The model that was used in this study, including the script to reproduce the data from (Simon et al., 2017) are openly available in github at https://doi.org/10.5281/zenodo.8100980

References

Adams, C., Gentry, A., Whybrow, P.J., 1983. Dating the terminal Tethyan event. Utrecht Micropaleontol. Bull. 30, 273–298.

Alhammoud, B., Meijer, P.T., Dijkstra, H.A., 2010. Sensitivity of Mediterranean thermohaline circulation to gateway depth: a model investigation. Paleoceanography 25 (2).

Astraldi, M., Balopoulos, S., Candela, J., Font, J., Gacic, M., Gasparini, G., Manca, B., Theocharis, A., Tintoré, J., 1999. The role of straits and channels in understanding the characteristics of Mediterranean circulation. Prog. Oceanogr. 44 (1–3), 65–108.
Barrier, E., Vrielynck, B., 2008. Palaeotectonic Maps of the Middle East. Atlas of, p. 14.
Benson, R., Rakic-El Beid, K., Bonaduce, G., 1992. An important current reversal (influx) in the Rifian corridor (Morocco) at the Tortonian-Messinian boundary: the end of Tethys Ocean. Notes et mémoires du Serv. Géol. 366, 115–146.
Bergamasco, A., Malanotte-Rizzoli, P., 2010. The circulation of the Mediterranean Sea: a historical review of experimental investigations. Adv. Oceanogr. Limnol. 1 (1), 11–28.
Besiou, E., Kontakiotis, G., Antonarakou, A., Mulch, A., Vasiliev, I., 2021. Climate and carbon cycle changes drive the hydrographic configuration of the eastern Mediterranean through the Tortonian-Messinian Transition. In: EGU General Assembly Conference Abstracts.
Bijma, J., Faber, W.W., Hemleben, C., 1990. Temperature and salinity limits for growth and survival of some planktonic foraminifers in laboratory cultures. J. Foraminiferal Res. 20 (2), 95–116.
Blanc, P.-L., Duplessy, J.-C., 1982. The deep-water circulation during the Neogene and the impact of the Messinian salinity crisis. Deep Sea Res. Part A. Oceanograp. Res. Papers 29 (12), 1391–1414.
Blanc-Valleron, M.-M., Pierre, C., Caulet, J., Caruso, A., Rouchy, J.-M., Cespuglio, G., Sprovieri, R., Pestrea, S., Di Stefano, E., 2002. Sedimentary, stable isotope and micropaleontological records of paleoceanographic change in the Messinian Tripoli Formation (Sicily, Italy). Palaeogeogr. Palaeoclimatol. Palaeoecol. 185 (3–4), 255–286.
Booth-Rea, G., Ranero, C.R., Grevemeyer, I., 2018. The Alboran volcanic-arc modulated the Messinian faunal exchange and salinity crisis. Sci. Rep. 8 (1), 13015.
Bryden, H.L., Kinder, T.H., 1991. Steady two-layer exchange through the Strait of Gibraltar. *Deep Sea Research Part a*. Oceanograph. Res. Paper. 38, S445–S463.
Bulian, F., Sierro, F.J., Ledesma, S., Jiménez-Espejo, F.J., Bassetti, M.-A., 2021. Messinian West Alboran Sea record in the proximity of Gibraltar: early signs of Atlantic-Mediterranean gateway restriction. Mar. Geol. 106430.
Bulian, F., Kouwenhoven, T.J., Jiménez-Espejo, F.J., Krijgsman, W., Andersen, N., Sierro, F.J., 2022. Impact of the Mediterranean-Atlantic connectivity and the late miocene carbon shift on deep-sea communities in the Western Alboran Basin. Palaeogeogr. Palaeoclimatol. Palaeoecol. 110841.
Butiseacă, G.A., Van der Meer, M.T., Kontakiotis, G., Agiadi, K., Thivaiou, D., Besiou, E., Antonarakou, A., Mulch, A., Vasiliev, I., 2022. Multiple crises preceded the Mediterranean Salinity Crisis: Aridification and vegetation changes revealed by biomarkers and stable isotopes. Glob. Planet. Chang. 217, 103951.
Candela, J., 1991. The Gibraltar Strait and its role in the dynamics of the Mediterranean Sea. Dyn. Atmos. Oceans 15 (3–5), 267–299.
Capella, W., Barhoun, N., Flecker, R., Hilgen, F., Kouwenhoven, T., Matenco, L., Sierro, F. J., Tulbure, M., Yousfi, M.Z., Krijgsman, W., 2018. Palaeogeographic evolution of the late Miocene Rifian Corridor (Morocco): reconstructions from surface and subsurface data. Earth Sci. Rev. 180, 37–59.
CIESM, 2008. The Messinian salinity crisis from mega-deposits to microbiology. In: Briand, F. (Ed.), A Consensus Report, in 33ème CIESM Workshop Monographs, 33. CIESM, 16, Bd de Suisse, MC-98000, Monaco, pp. 1–168.
Conroy, J.L., Thompson, D.M., Cobb, K.M., Noone, D., Rea, S., Legrande, A.N., 2017. Spatiotemporal variability in the δ18O-salinity relationship of seawater across the tropical Pacific Ocean. Paleoceanography 32 (5), 484–497.
Corbí, H., Soria, J.M., Giannetti, A., Yébenes, A., 2020a. The step-by-step restriction of the Mediterranean (start, amplification, and consolidation phases) preceding the Messinian Salinity Crisis (climax phase) in the Bajo Segura basin. Geo-Mar. Lett. 40 (3), 1–21.
Corbí, H., Soria, J.M., Giannetti, A., Yébenes, A., 2020b. The step-by-step restriction of the Mediterranean (start, amplification, and consolidation phases) preceding the Messinian Salinity Crisis (climax phase) in the Bajo Segura basin. Geo-Mar. Lett. 1–21.
De La Vara, A., Topper, R.P., Meijer, P.T., Kouwenhoven, T.J., 2015. Water exchange through the Betic and Rifian corridors prior to the Messinian Salinity Crisis: a model study. Paleoceanography 30 (5), 548–557.
de Weger, W., Hernández-Molina, F.J., Flecker, R., Sierro, F.J., Chiarella, D., Krijgsman, W., Manar, M.A., 2020. Late Miocene contourite channel system reveals intermittent overflow behavior. Geology 48 (12), 1194–1199.
De Weger, W., Hernández-Molina, F.J., Miguez-Salas, O., De Castro, S., Bruno, M., Chiarella, D., Sierro, F.J., Blackbourn, G., Manar, M.A., 2021. Contourite depositional system after the exit of a strait: Case study from the late Miocene South Rifian Corridor, Morocco. Sedimentology 68 (7), 2996–3032.
Di Stefano, A., Verducci, M., Lirer, F., Ferraro, L., Iaccarino, S.M., Hüsing, S.K., Hilgen, F. J., 2010. Paleoenvironmental conditions preceding the Messinian Salinity Crisis in the Central Mediterranean: integrated data from the Upper Miocene Trave section (Italy). Palaeogeogr. Palaeoclimatol. Palaeoecol. 297 (1), 37–53.
Dirksen, J.P., Meijer, P., 2020. The mechanism of sapropel formation in the Mediterranean Sea: insight from long-duration box model experiments. Clim. Past 16 (3), 933–952.
Drinia, H., Antonarakou, A., Tsaparas, N., Kontakiotis, G., 2007. Palaeoenvironmental conditions preceding the Messinian Salinity Crisis: a case study from Gavdos Island. Geobios 40 (3), 251–265.
Ebner, R., & Meijer, P. T. (In prep.) 2024.
Fadil, A., Vernant, P., McClusky, S., Reilinger, R., Gomez, F., Ben Sari, D., Mourabit, T., Feigl, K., Barazangi, M., 2006. Active tectonics of the western Mediterranean: Geodetic evidence for rollback of a delaminated subcontinental lithospheric slab beneath the Rif Mountains, Morocco. Geology 34 (7), 529–532.
Filippelli, G.M., Sierro, F.J., Flores, J.A., Vázquez, A., Utrilla, R., Pérez-Folgado, M., Latimer, J.C., 2003. A sediment–nutrient–oxygen feedback responsible for productivity variations in late Miocene sapropel sequences of the western Mediterranean. Palaeogeogr. Palaeoclimatol. Palaeoecol. 190, 335–348. https://doi.org/10.1016/s0031-0182(02)00613-2.
Flecker, R., Krijgsman, W., Capella, W., De Castro Martíns, C., Dmitrieva, E., Mayser, J. P., Marzocchi, A., Modestou, S., Ochoa, D., Simon, D., Tulbure, M., Van Den Berg, B., Van Der Schee, M., De Lange, G., Ellam, R., Govers, R., Gutjahr, M., Hilgen, F., Kouwenhoven, T., Yousfi, M.Z., 2015. Evolution of the Late Miocene Mediterranean–Atlantic gateways and their impact on regional and global environmental change. Earth Sci. Rev. 150, 365–392. https://doi.org/10.1016/j.earscirev.2015.08.007.
Fortuin, A., Krijgsman, W., 2003. The Messinian of the Nijar Basin (SE Spain): sedimentation, depositional environments and paleogeographic evolution. Sediment. Geol. 160 (1–3), 213–242.
Garcia-Castellanos, D., Villaseñor, A., 2011. Messinian salinity crisis regulated by competing tectonics and erosion at the Gibraltar arc. Nature 480 (7377), 359.
Govers, R., 2009. Choking the Mediterranean to dehydration: the Messinian salinity crisis. Geology 37 (2), 167–170.
Herbert, T.D., Lawrence, K.T., Tzanova, A., Peterson, L.C., Caballero-Gill, R., Kelly, C.S., 2016. Late Miocene global cooling and the rise of modern ecosystems. Nat. Geosci. 9 (11), 843–847.
Hilgen, F., Krijgsman, W., Langereis, C., Lourens, L., Santarelli, A., Zachariasse, W., 1995. Extending the astronomical (polarity) time scale into the Miocene. Earth Planet. Sci. Lett. 136 (3–4), 495–510.
Holbourn, A.E., Kuhnt, W., Clemens, S.C., Kochhann, K.G., Jöhnck, J., Lübbers, J., Andersen, N., 2018. Late Miocene climate cooling and intensification of southeast Asian winter monsoon. Nat. Commun. 9 (1), 1584.
Hüsing, S., Kuiper, K., Link, W., Hilgen, F.J., Krijgsman, W., 2009. The upper Tortonian–lower Messinian at Monte Dei Corvi (Northern Apennines, Italy): completing a Mediterranean reference section for the Tortonian stage. Earth Planet. Sci. Lett. 282 (1–4), 140–157.
Hüsing, S., Oms, O., Agustí, J., Garcés, M., Kouwenhoven, T., Krijgsman, W., Zachariasse, W.-J., 2010. On the late Miocene closure of the Mediterranean–Atlantic gateway through the Guadix basin (southern Spain). Palaeogeogr. Palaeoclimatol. Palaeoecol. 291 (3–4), 167–179.
Karakitsios, V., Cornée, J.-J., Tsourou, T., Moissette, P., Kontakiotis, G., Agiadi, K., Manoutsoglou, E., Triantaphyllou, M., Koskeridou, E., Drinia, H., 2017a. Messinian salinity crisis record under strong freshwater input in marginal, intermediate, and deep environments: the case of the North Aegean. Palaeogeogr. Palaeoclimatol. Palaeoecol. 485, 316–335.
Karakitsios, V., Roveri, M., Lugli, S., Manzi, V., Gennari, R., Antonarakou, A., Triantaphyllou, M., Agiadi, K., Kontakiotis, G., Kafousia, N., 2017b. A record of the Messinian salinity crisis in the eastern Ionian tectonically active domain (Greece, eastern Mediterranean). Basin Res. 29 (2), 203–233.
Knudsen, M., 1900. Ein hydrographischer lehrsatz. Ann. Hydrogr. Marit. Meteorol. 28 (7), 316–320.
Kontakiotis, G., Besiou, E., Antonarakou, A., Zarkogiannis, S., Kostis, A., Mortyn, P., Moissette, P., Cornée, J.-J., Schulbert, C., Drinia, H., 2019. Decoding Sea surface and paleoclimate conditions in the eastern Mediterranean over the Tortonian-Messinian transition. Palaeogeogr. Palaeoclimatol. Palaeoecol. 534, 109312.
Kontakiotis, G., Butiseacă, G.A., Antonarakou, A., Agiadi, K., Zarkogiannis, S.D., Krsnik, E., Besiou, E., Zachariasse, W.J., Lourens, L., Thivaiou, D., 2022. Hypersalinity accompanies tectonic restriction in the eastern Mediterranean prior to the Messinian Salinity Crisis. Palaeogeogr. Palaeoclimatol. Palaeoecol. 592, 110903.
Kouwenhoven, T., Seidenkrantz, M.-S., Van der Zwaan, G., 1999. Deep-water changes: the near-synchronous disappearance of a group of benthic foraminifera from the late Miocene Mediterranean. Palaeogeogr. Palaeoclimatol. Palaeoecol. 152 (3–4), 259–281.
Kouwenhoven, T., Hilgen, F., Van der Zwaan, G., 2003a. Late Tortonian–early Messinian stepwise disruption of the Mediterranean–Atlantic connections: constraints from benthic foraminiferal and geochemical data. Palaeogeogr. Palaeoclimatol. Palaeoecol. 198 (3–4), 303–319.
Kouwenhoven, T.J., Hilgen, F.J., Van Der Zwaan, G.J., 2003b. Late Tortonian–early Messinian stepwise disruption of the Mediterranean–Atlantic connections: constraints from benthic foraminiferal and geochemical data. Palaeogeogr. Palaeoclimatol. Palaeoecol. 198 (3–4), 303–319. https://doi.org/10.1016/s0031-0182(03)00472-3.
Kouwenhoven, T., Morigi, C., Negri, A., Giunta, S., Krijgsman, W., Rouchy, J.-M., 2006. Paleoenvironmental evolution of the eastern Mediterranean during the Messinian: Constraints from integrated microfossil data of the Pissouri Basin (Cyprus). Mar. Micropaleontol. 60 (1), 17–44.
Krijgsman, W., Meijer, P.T., 2008. Depositional environments of the Mediterranean "lower Evaporites" of the Messinian salinity crisis: Constraints from quantitative analyses. Mar. Geol. 253 (3–4), 73–81.
Krijgsman, W., Hilgen, F., Langereis, C., Zachariasse, W., 1994. The age of the Tortonian/Messinian boundary. Earth Planet. Sci. Lett. 121, 533–547.
Krijgsman, W., Hilgen, F., Negri, A., Wijbrans, J., Zachariasse, W., 1997. The Monte del Casino section (northern Apennines, Italy): a potential Tortonian/Messinian boundary stratotype? Palaeogeogr. Palaeoclimatol. Palaeoecol. 133 (1–2), 27–47.
Krijgsman, W., Langereis, C., Zachariasse, W., Boccaletti, M., Moratti, G., Gelati, R., Iaccarino, S., Papani, G., Villa, G., 1999. Late Neogene evolution of the Taza–Guercif Basin (Rifian Corridor, Morocco) and implications for the Messinian salinity crisis. Mar. Geol. 153 (1–4), 147–160.

Krijgsman, W., Garcés, M., Agustı, J., Raffi, I., Taberner, C., Zachariasse, W., 2000. The 'Tortonian salinity crisis' of the eastern Betics (Spain). Earth Planet. Sci. Lett. 181 (4), 497–511.
Krijgsman, W., Stoica, M., Vasiliev, I., Popov, V.V., 2010. Rise and fall of the Paratethys Sea during the Messinian Salinity Crisis, 290 (1–2), 183–191. https://doi.org/10.1016/j.epsl.2009.12.020.
Lacombe, H., Richez, C., 1982. The regime of the Strait of Gibraltar. In: Elsevier Oceanography Series, vol. 34. Elsevier, pp. 13–73.
Laskar, J., Robutel, P., Joutel, F., Gastineau, M., Correia, A.C., Levrard, B., 2004. A long-term numerical solution for the insolation quantities of the Earth. Astron. Astrophys. 428 (1), 261–285.
Lirer, F., Foresi, L.M., Iaccarino, S.M., Salvatorini, G., Turco, E., Cosentino, C., Sierro, F. J., Caruso, A., 2019. Mediterranean Neogene planktonic foraminifer biozonation and biochronology. Earth Sci. Rev. 196, 102869.
Lofi, J., Déverchère, J., Gaullier, V., Gillet, H., Gorini, C., Guennoc, P., Loncke, L., Maillard, A., Sage, F., Thinon, I., 2011. Seismic Atlas of the Messinian Salinity Crisis Markers in the Mediterranean and Black Seas, vol. 179. Société Géologique de France.
Mancilla, F.D.L., Booth-Rea, G., Stich, D., Pérez-Peña, J.V., Morales, J., Azañón, J.M., Martin, R., Giaconia, F., 2015. Slab rupture and delamination under the Betics and Rif constrained from receiver functions. Tectonophysics 663, 225–237.
Martín, J.M., Braga, J.C., Sánchez-Almazo, I., 1999. 43. The Messinian Recordofthe Outcropping Marginal Alboran BASIN DEPOSITS: SIGNIFICANCE AND Implications1.
Matthiesen, S., Haines, K., 2003. A hydraulic box model study of the Mediterranean response to postglacial sea-level rise. Paleoceanography 18 (4).
Meijer, P.T., 2006. A box model of the blocked-outflow scenario for the Messinian Salinity Crisis. Earth Planet. Sci. Lett. 248 (1–2), 486–494.
Meijer, P.T., 2012. Hydraulic theory of sea straits applied to the onset of the Messinian Salinity Crisis. Mar. Geol. 326, 131–139.
Meijer, P., 2021. (Paleo) oceanography of semi-enclosed seas with a focus on the Mediterranean region; Insights from basic theory. Earth Sci. Rev. 221, 103810.
Meijer, P.T., Slingerland, R., Wortel, M., 2004. Tectonic control on past circulation of the Mediterranean Sea: a model study of the late Miocene. Paleoceanography 19 (1).
Moissette, P., Cornée, J.-J., Antonarakou, A., Kontakiotis, G., Drinia, H., Koskeridou, E., Tsourou, T., Agiadi, K., Karakitsios, V., 2018. Palaeoenvironmental changes at the Tortonian/Messinian boundary: a deep-sea sedimentary record of the eastern Mediterranean Sea. Palaeogeogr. Palaeoclimatol. Palaeoecol. 505, 217–233.
Morigi, C., 2009. Benthic environmental changes in the Eastern Mediterranean Sea during sapropel S5 deposition. Palaeogeogr. Palaeoclimatol. Palaeoecol. 273 (3–4), 258–271.
Morigi, C., Jorissen, F., Gervais, A., Guichard, S., Borsetti, A., 2001. Benthic foraminiferal faunas in surface sediments off NW Africa: relationship with organic flux to the ocean floor. J. Foraminifer. Res. 31 (4), 350–368.
Morigi, C., Negri, A., Giunta, S., Kouwenhoven, T., Krijgsman, W., Blanc-Valleron, M.-M., Orszag-Sperber, F., Rouchy, J.-M., 2007. Integrated quantitative biostratigraphy of the latest Tortonian–early Messinian Pissouri section (Cyprus): an evaluation of calcareous plankton bioevents. Geobios 40 (3), 267–279.
Nijenhuis, I., Schenau, S., Van der Weijden, C., Hilgen, F., Lourens, L., Zachariasse, W., 1996. On the origin of upper Miocene sapropelites: a case study from the Faneromeni section, Crete (Greece). Paleoceanography 11 (5), 633–645.
Rio, D., Silva, I.P., Capraro, L., 2003. The geologic time scale and the Italian stratigraphic record. Episod. J. Int. Geosci. 26 (3), 259–263.
Rogerson, M., Rohling, E., Bigg, G.R., Ramirez, J., 2012. Paleoceanography of the Atlantic-Mediterranean exchange: Overview and first quantitative assessment of climatic forcing. Rev. Geophys. 50 (2).
Rögl, F., 1999. Mediterranean and Paratethys. Facts and hypotheses of an Oligocene to Miocene paleogeography (short overview). Geol. Carpath. 50 (4), 339–349.
Rohling, E., Marino, G., Grant, K., 2015. Mediterranean climate and oceanography, and the periodic development of anoxic events (sapropels). Earth Sci. Rev. 143, 62–97.
Rouchy, J.-M., Pierre, C., Et-Touhami, M., Kerzazi, K., Caruso, A., Blanc-Valleron, M.-M., 2003. Late Messinian to early Pliocene paleoenvironmental changes in the Melilla Basin (NE Morocco) and their relation to Mediterranean evolution. Sediment. Geol. 163 (1–2), 1–27.
Roveri, M., Flecker, R., Krijgsman, W., Lofi, J., Lugli, S., Manzi, V., Sierro, F.J., Bertini, A., Camerlenghi, A., De Lange, G., 2014. The Messinian Salinity Crisis: past and future of a great challenge for marine sciences. Mar. Geol. 352, 25–58.
Santarelli, A., Brinkhuis, H., Hilgen, F., Lourens, L., Versteegh, G., Visscher, H., 1998. Orbital signatures in a Late Miocene dinoflagellate record from Crete (Greece). Mar. Micropaleontol. 33 (3–4), 273–297.
Santisteban, C., Taberner, C., 1983. Shallow marine and continental conglomerates derived from coral reef complexes after desiccation of a deep marine basin: the Tortonian-Messinian deposits of the Fortuna Basin, SE Spain. J. Geol. Soc. Lond. 140 (3), 401–411.
Schenau, S., Antonarakou, A., Hilgen, F., Lourens, L., Nijenhuis, I., Van der Weijden, C., Zachariasse, W., 1999. Organic-rich layers in the Metochia section (Gavdos, Greece): evidence for a single mechanism of sapropel formation during the past 10 my. Mar. Geol. 153 (1–4), 117–135.
Seidenkrantz, M.-S., Kouwenhoven, T., Jorissen, F., Shackleton, N., Van der Zwaan, G., 2000. Benthic foraminifera as indicators of changing Mediterranean–Atlantic water exchange in the late Miocene. Mar. Geol. 163 (1–4), 387–407.
Selli, R., 1964. The Mayer-Eymar Messinian 1867. Proposal for a neostratotype. In: Proc. 21st IGC Copenhagen 1960, 28, pp. 311–333.
Sierro, F.J., Flores, J.A., Francés, G., Vazquez, A., Utrilla, R., Zamarreño, I., Erlenkeuser, H., Barcena, M.A., 2003. Orbitally-controlled oscillations in planktic communities and cyclic changes in western Mediterranean hydrography during the Messinian [Conference Paper]. Palaeogeogr. Palaeoclimatol. Palaeoecol. 190, 289–316. https://doi.org/10.1016/S0031-0182(02)00611-9.
Simon, D., Meijer, P., 2015. Dimensions of the Atlantic–Mediterranean connection that caused the Messinian Salinity Crisis. Mar. Geol. 364, 53–64.
Simon, D., Meijer, P.T., 2017. Salinity stratification of the Mediterranean Sea during the Messinian crisis: a first model analysis. Earth Planet. Sci. Lett. 479, 366–376.
Simon, D., Marzocchi, A., Flecker, R., Lunt, D.J., Hilgen, F.J., Meijer, P.T., 2017. Quantifying the Mediterranean freshwater budget throughout the late Miocene: New implications for sapropel formation and the Messinian Salinity Crisis. Earth Planet. Sci. Lett. 472, 25–37.
Sprovieri, R., Di Stefano, E., Caruso, A., Bonomo, S., 1996a. High resolution stratigraphy in the Messinian Tripoli Formation in Sicily. Paleopelagos 6, 415–435.
Sprovieri, R., Di Stefano, E., Sprovieri, M., 1996b. High resolution chronology for late Miocene Mediterranean stratigraphic events. Riv. Ital. Paleontol. Stratigr. 102 (1).
Sprovieri, M., Bellanca, A., Neri, R., Mazzola, S., Bonanno, A., Patti, B., Sorgente, R., 1999. Astronomical calibration of late Miocene stratigraphic events and analysis of precessionally driven paleoceanographic changes in the Mediterranean basin. Mem. Soc. Geol. Ital. 54, 7–24.
Stoica, M., Krijgsman, W., Fortuin, A., Gliozzi, E., 2016. Paratethyan ostracods in the Spanish Lago-Mare: more evidence for interbasinal exchange at high Mediterranean Sea level. Palaeogeogr. Palaeoclimatol. Palaeoecol. 441, 854–870.
Topper, R., Meijer, P., 2014. A high resolution ocean model of restriction of the Mediterranean-Atlantic connection: changes in Mediterranean circulation and water characteristics. In: EGU General Assembly Conference Abstracts.
Topper, R., Meijer, P.T., 2015. Changes in Mediterranean circulation and water characteristics due to restriction of the Atlantic connection: a high-resolution ocean model. Clim. Past 11 (2), 233–251.
Tulbure, M., Capella, W., Barhoun, N., Flores, J., Hilgen, F., Krijgsman, W., Kouwenhoven, T., Sierro, F.J., Yousfi, M.Z., 2017. Age refinement and basin evolution of the North Rifian Corridor (Morocco): no evidence for a marine connection during the Messinian Salinity Crisis. Palaeogeogr. Palaeoclimatol. Palaeoecol. 485, 416–432.
Tziperman, E., Speer, K., 1994. A study of water mass transformation in the Mediterranean Sea: analysis of climatological data and a simple three-box model. Dyn. Atmos. Oceans 21 (2–3), 53–82.
Van Assen, E., Kuiper, K., Barhoun, N., Krijgsman, W., Sierro, F., 2006. Messinian astrochronology of the Melilla Basin: stepwise restriction of the Mediterranean–Atlantic connection through Morocco. Palaeogeogr. Palaeoclimatol. Palaeoecol. 238 (1–4), 15–31.
Van den Berg, B.C.J., Sierro, F.J., Hilgen, F.J., Flecker, R., Larrasoaña, J.C., Krijgsman, W., Flores, J.A., Mata, M.P., 2018. Imprint of Messinian Salinity Crisis events on the Spanish Atlantic margin. Newsl. Stratigr. 51 (1), 93–115. https://doi.org/10.1127/nos/2017/0337.
Van Der Laan, E., Hilgen, F.J., Lourens, L.J., De Kaenel, E., Gaboardi, S., Iaccarino, S., 2012. Astronomical forcing of Northwest African climate and glacial history during the late Messinian (6.5–5.5Ma). Palaeogeogr. Palaeoclimatol. Palaeoecol. 313-314, 107–126. https://doi.org/10.1016/j.palaeo.2011.10.013.
Van Der Schee, M., Sierro, F.J., Jiménez-Espejo, F.J., Hernández-Molina, F.J., Flecker, R., Flores, J.A., Acton, G., Gutjahr, M., Grunert, P., García-Gallardo, Á., Andersen, N., 2016. Evidence of early bottom water current flow after the Messinian Salinity Crisis in the Gulf of Cadiz, 380, 315–329. https://doi.org/10.1016/j.margeo.2016.04.005.
Vasiliev, I., Karakitsios, V., Bouloubassi, I., Agiadi, K., Kontakiotis, G., Antonarakou, A., Triantaphyllou, M., Gogou, A., Kafousia, N., de Rafélis, M., 2019. Large sea surface temperature, salinity, and productivity-preservation changes preceding the onset of the Messinian Salinity Crisis in the eastern Mediterranean Sea. Paleoceanograph. Paleoclimatol. 34 (2), 182–202.
Vázquez, A., Utrilla, R., Zamarreno, I., Sierro, F., Flores, J., Francés, G., Barcena, M., 2000. Precession-related sapropelites of the Messinian Sorbas Basin (South Spain): paleoenvironmental significance. Palaeogeogr. Palaeoclimatol. Palaeoecol. 158 (3–4), 353–370.
Violanti, D., Lozar, F., Natalicchio, M., Dela Pierre, F., Bernardi, E., Clari, P., Cavagna, S., 2013. Stress-tolerant microfossils of a Messinian succession from the Northern Mediterranean basin (Pollenzo section, Piedmont, northwestern Italy). Boll. Soc. Paleontol. Ital. 52 (1), 46.
Waldman, R., Brüggemann, N., Bosse, A., Spall, M., Somot, S., Sevault, F., 2018. Overturning the Mediterranean thermohaline circulation. Geophys. Res. Lett. 45 (16), 8407–8415.
Zachariasse, W.J., Lourens, L.J., 2022. The Messinian on Gavdos (Greece) and the status of currently used ages for the onset of the MSC and gypsum precipitation. Newsl. Stratigr. 55 (3), 333–360.
Zachariasse, W.J., Kontakiotis, G., Lourens, L.J., Antonarakou, A., 2021. The Messinian of Agios Myron (Crete, Greece): a key to better understanding of diatomite formation on Gavdos (south of Crete). Palaeogeogr. Palaeoclimatol. Palaeoecol. 581, 110633.